European Journal of Applied Sciences – Vol. 13, No. 02
Publication Date: April 25, 2025
DOI:10.14738/aivp.1302.18421.
Yang, C.-C., Vien, T. T. T., & Lin, Y.-S. (2025). The Cold Forming Analysis of Stainless Battery Bolts. European Journal of Applied Sciences, Vol - 13(02). 72-83.

The Cold Forming Analysis of Stainless Battery Bolts

Chih-Cheng Yang
Department of Mechanical and Automation Engineering,
Taiwan Steel University, Taiwan

Thi Thu Trang Vien
Graduate School of Mechatronic Science
and Technology, Taiwan Steel University, Taiwan

Yung-Sheng Lin
Graduate School of Mechatronic Science
and Technology, Taiwan Steel University, Taiwan

ABSTRACT

A multi-stage cold forming process for the manufacture of stainless battery bolts is studied numerically with AISI 316 stainless steel in this study. The cold forming process through five stages includes preparation and centering for backward extrusion, backward extrusion over a die pin, two upsetting operations, and square trimming. The numerical simulations of cold forming are carried out using the finite element code of DEFORM-3D. The formability of the workpiece is studied, such as the effect on forming force responses, maximum forming forces, effective stress and strain distributions and metal flow pattern. In the five-stage forming process, in the two upsetting and the square trimming forming stages, the effective stresses in the head of the workpiece are significantly high, and the effective strains are also significantly high due to large deformation. The flow line distributions are also very complex in which the flow lines in the trimming region of the upset head are severely bent, highly compacted, and eventually fractured due to excessive trimming. For the maximum axial forming force, the fourth stage of secondary upsetting to form a cylindrical head to a larger outer diameter is 347.2 kN, which is the largest among the five stages due to the large amount of upsetting. However, for the forming energy, the third stage, which the workpiece is firstly upset into a conical shape, is 530.1 J, which is the largest among the five stages due to longer acted axial forming stroke. The total maximum axial forming forces from the first to the last stages are 597.1 kN and the total forming energies are about 1.36 kJ.

Keywords: cold forming, stainless battery bolt, square trimming, formability, forming force.

1. INTRODUCTION

Cold forming processes are performed at room temperature and widely used in the manufacture of various parts. Multi-stage cold forming is used in many industries, especially in the manufacture of fasteners and special parts. High mechanical properties, good surface appearance and good precision are usually achieved without further processing. Multi-stage

cold forming is a high-speed forming process in which the billet is formed sequentially through multiple stations [1].

In the cold forming process, the prediction of forming forces and stresses is significance for the design of punches and dies and the selection of forming machines. There are many cold forming applications that use numerical simulation to predict and analyze the forming design. Altan and Knoerr [2] applied two-dimensional finite element method to study suck-in type extrusion defects, bevel gear forging, stress analysis of forging tools and multi-stage cold forging design. Lee et al. [3] used the rigid-plastic finite element method to design a multi-stage cold forging process sequence to form a constant velocity joint housing with shaft. They studied velocity distributions, effective strain distributions, and forging loads, which provided useful information in process design. A numerical simulation technique for the forging process with a spring-attached die was proposed by Joun et al. [4], which used a penalty rigid-viscoplastic finite element method with an iterative force balance method. They explored the significance of metal flow lines on quality control and the influence of spring-attached dies on metal flow lines and forming load reduction. Roque and Button [5] applied ANSYS commercial finite element software to model a forming operation. They developed models to simulate ring compression testing and upsetting operations, a stage in the manufacturing process for automotive starter parts.

MacCormack and Monaghan [6] proposed a three-stage cold forming process to form the spline shape of the head of aerospace fasteners. They gained insight into the operation by numerically analyzing strain, damage, and flow patterns in three stages. To analyze the formability of the multi-stage forming process, Park et al. [7] used the finite element method to establish a systematic process analysis method for the multi-stage forming of the constant velocity joint outer ring. Farhoumand and Ebrahimi [8] applied the FE code of ABAQUS to analyze the forward-backward-radial extrusion process and studied the effects of geometric parameters such as die corner radius and gap height as well as process conditions such as friction on the process. The numerical results were compared with experimental data in terms of forming loads and material flow lines in different regions. The hardness distribution of the longitudinal section of the product was used to verify the strain distributions obtained by numerical analysis. Jafarzadeh et al. [9] applied the DEFORM-3D finite element code to study the lateral extrusion process and analyzed the influence of some important geometric parameters such as initial billet dimensions, gap height and friction conditions on the required forging loads, material flow patterns and effective strain distributions. This study analyzed and compared 4 and 5 stages of fasteners. They used the DEFORM-3D FE code to inspect the effective stresses, strains, and velocities from billet to finished product. An application of finite element analysis in the prediction and optimization of bolt forming process was presented by Paćko et al. [10]. They studied bolt forming process consists of six stages, including shearing, three upsetting stages, backward extrusion, and trimming. Several tool modifications were proposed and analyzed using numerical simulation. Yang and Lin [11] conducted numerical and experimental investigations on two forming modes of two-step extrusion of AISI 1010 carbon steel. The numerical results of effective strain distributions were consistent with the experimentally measured hardness distributions.

Ku [12] proposed a two-stage cold forging process for manufacturing AISI 1035 steel drive shaft with internal spline and spur gear geometry. Francy et al. [13] used DEFORM-3D software and Taguchi method to optimize the input process parameters in the extrusion process. The simulations were performed using DFORM-3D software to predict the minimum force achieved in cold forward extrusion process. Obiko et al. [14] applied DEFORM 3D to perform three-dimensional finite element analysis to study the plastic deformation behavior of X20CrMoV121 steel during forging process. They studied the effect of forging temperature on the strain, stress and particle flow velocity distribution during forging process. Petkar et al. [15] proposed the use of a multi-layer feed-forward artificial neural network (ANN) model to determine the effects of process parameters such as billet size, reduction ratio, punch angle and land height on the cold forging backward extrusion forming behavior (i.e., effective stress, strain, strain rate and punch force) of AISI 1010 steel. Finite element simulation along with the developed artificial neural network model scheme could help the cold forging industry to minimize the cost and time of process development. Lee et al. [16] proposed the use of a multi-stage cold forging process to reduce the manufacturing cost of the solenoid valve while meeting dimensional accuracy and performance. The forming process is divided into six stages to improve the dimensional accuracy of the armature outer diameter, overall length and slot portion.

Yang and Liu [17] conducted numerical and experimental investigations on a five-stage cold forming process of mild steel AISI 1010 relief valve regulating nuts. The numerical simulation of the forming force growth tendency was consistent with the experimental results. The effective strain distributions were consistent with the measured hardness distributions. The highly compact grain flow lines also led to higher hardness. Yang et al. [18] conducted a numerical study on the multi-stage cold forming process for manufacturing eccentric parts of mild steel AISI 1022. The formability of the workpiece was numerically investigated, such as the effect on forging load responses, maximum forging loads, effective stress and strain distributions, and metal flow patterns. Although the total maximum axial forging load of four-stage forming was less than that of five-stage forming, the maximum lateral forging force in the last stage of four-stage forming was almost 5 times that of the last stage of five-stage forming. Increasing the lateral forging force might cause wear and damage to the punch. Tao et al. [19] aimed to determine an appropriate cold forging process for thin-walled A286 super alloy tube with ideal forming quality. The effects of two forging processes using reverse forging sequence on the forming defects and hardness distribution of thin-walled tubes were analyzed through finite element simulation. Based on the three-dimensional finite element model, Wan et al. [20] analyzed the residual stress distribution around the cold extrusion internal thread of 42CrMo4 high-strength steel plate hole structure under different edge distance ratios. They established the multi-axial fatigue life prediction model of thread based on the stress-strain method and the accuracy and feasibility of the prediction model were further verified by fatigue experiments. The research showed that the improved fatigue prediction model gave a satisfactory accuracy in predicting the fatigue life. Yang et al. [21] presented a numerical analysis of three-stage cold forming process for the manufacture of AISI 316 stainless steel Allen screws and hexalobular socket screws. In the three-stage forming process, in the forming stages of two upsetting and one backward extrusion at the upper face of the workpiece, the effective stresses in the head of the workpiece are significantly high, and the effective strains are also significantly high due to large deformation.

In the three-stage forming process, including two upsetting and one backward extrusion forming stages, the effective stresses at the upper face of the workpiece were significantly larger, and the effective strains were also larger due to the larger deformation. Winiarski et al. [22] proposed a new method for forming flanges in hollow parts. The process consisted of an extrusion with two dies that moved in an opposite direction to that of the punches. This particular kinematics of the tools made it possible to form two flanges simultaneously in a single tool pass.

In this study, the numerical simulation of a five-stage cold-forming process for the manufacture of AISI 316 stainless steel battery bolts is presented. The forming process includes preparation and centering for backward extrusion, backward extrusion over die pin, two upsetting operations, and square trimming. The numerical simulation of cold forming is conducted using the FE code of DEFORM-3D. The forming load responses are calculated and the metal flow pattern, effective stress and effective strain at various deformation zones are analyzed.

2. MATERIALS AND METHODS

The manufacturing process of the stainless battery bolts is multi-stage cold forming through five stages. A cold-forging quality AISI 316 stainless steel wire coil is used in the cold-forming analysis. The chemical composition of the alloy steel wire is shown in Table 1.

Table 1: Chemical composition of AISI 316 stainless steel wires (wt.%).

C	Mn	P	S	Si	Mo	Ni	Cr
0.08	2.0	0.043	0.025	1.0	2.5	10.0	16.0

The cold forming is numerically investigated using the finite element code of DEFORM-3D. A billet of ϕ5.85mm × L43.5mm is cut by the shearing die and transfers to forming stations. Figure 1 shows the three-dimensional and cross-section views for the initial billet and product parts at five stages.

Due to cutting to length by shearing, both the ends of the cutoff billet are visibly deformed, as shown in Figure 1. Therefore, the initial billet is no longer an axisymmetric cylindrical body. For the first stage, as shown in Figures 1(a) and 1(b), the process includes flattening the billet end and centering for the backward extrusion in the second stage. In the second stage, a cavity of ϕ3.0 mm is formed at the bottom end with a depth of 5.0 mm by using a punch tool mounted in the die and with a reduction in area of 25.6% for the backward extrusion. Then, the workpiece is moved to the third stage in which the upper end of the workpiece is upset into a conical shape, and then moved to the fourth stage where the workpiece is further upset into an approximately cylindrical shape with a height of 4 mm. In the final stage, the workpiece is trimmed into a thick square shape at the head. The deformation energy is

$$E = \int_0^{\Delta L} F dl \tag{1}$$

where F is forming force and ΔL is total acted forging stroke.

(a) 3D views

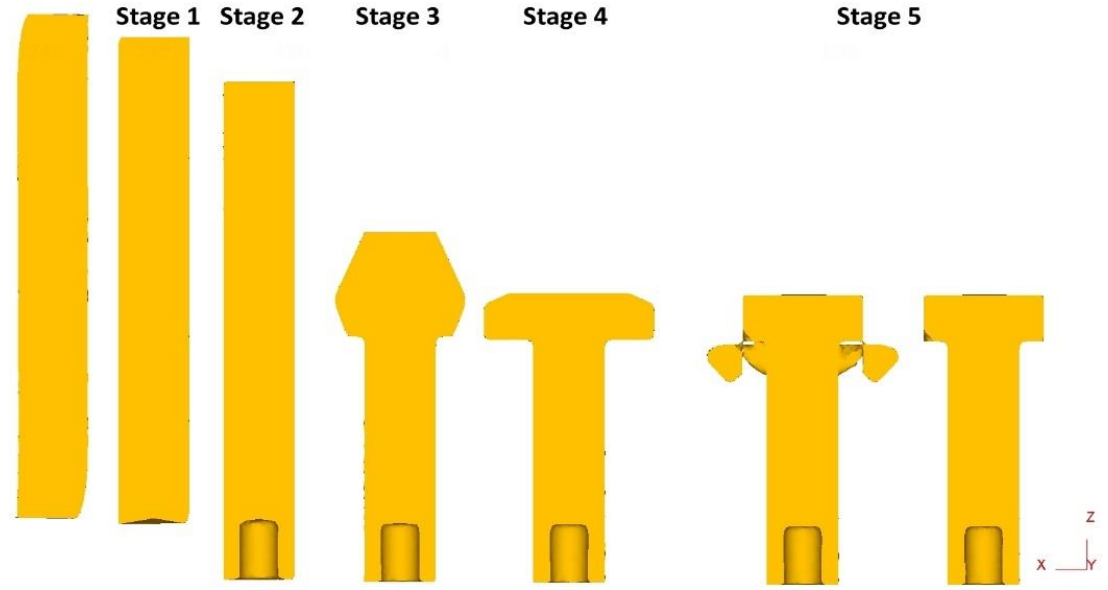

(b) cross-section views

Figure 1: The shapes for initial billet and product parts of each stage.

The numerical simulation of multi-stage cold forming is modeled as a 3D finite element analysis using DEFORM 3D. The workpiece is modeled using tetrahedral elements. The deformations of punches and dies are ignored and treated as rigid objects since their materials are usually much harder than the material of workpiece. The workpiece material is an AISI 316 stainless steel billet which is considered as a rigid-plastic material with Von Misses yield criterion, isotropic hardening. In order to obtain more accurate simulation result, a cylindrical compression test, with the specimens of ϕ8.0mm × L15.0mm, is conducted in a 20 tonne universal testing machine under a constant ram speed of 3 mm/min at room temperature, and the following equations are used to gain the true stress and true strain [23],

$$\sigma = P/A_0, \tag{2}$$

$$\varepsilon = (h - h_0)/h_0, \tag{3}$$

$$\sigma_t = \sigma\,(1 + \varepsilon) = \sigma\,(h/h_0), \tag{4}$$

$$\varepsilon_t = \ln(1 + \varepsilon) = \ln(h/h_0), \tag{5}$$

where σ is engineering stress, ε is engineering strain, P is compression force, A_0 is initial cross-sectional area, h_0 is initial height, h is the instantaneous height, σ_t is true stress and ε_t is true strain. Figure 2 shows the true stress-true strain diagram of AISI 316 stainless steel, which will be imported into the numerical code of DEFORM to conduct the forming simulation analysis.

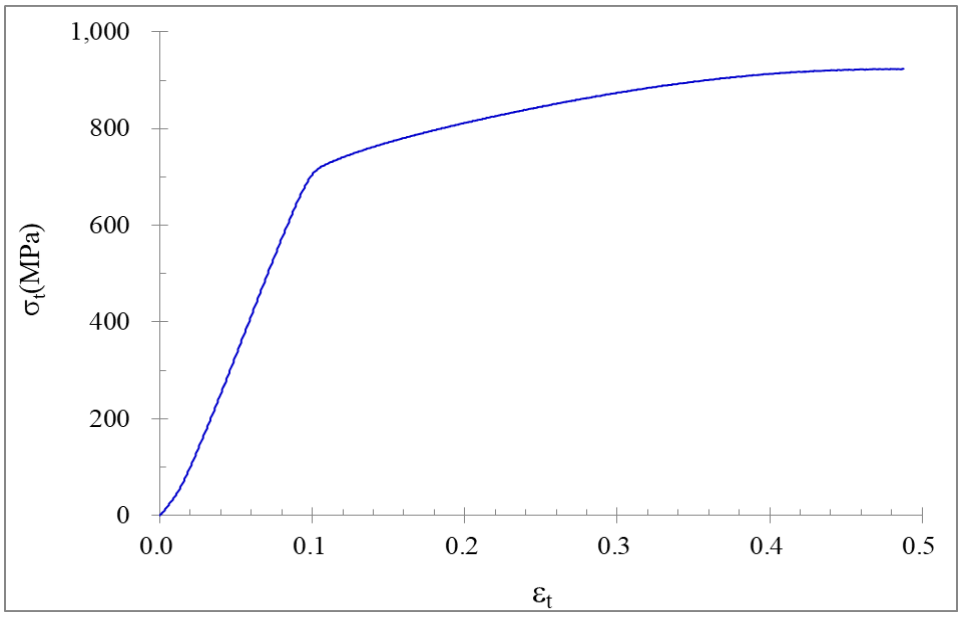

Figure 2: True stress-true train curve of AISI 316 stainless steel by compression test.

The friction between the workpiece and tools is considered as constant shear friction, and the friction coefficient for cold forming is m = 0.12. The relevant simulation settings are listed in Table 2.

Table 2: Simulation parameters in DEFORM.

Workpiece material	**AISI 316**
Workpiece/die property	Plastic/rigid
Temperature	20°C
Mesh number	42,000
Mesh element type	Tetrahedron
Friction model/friction coefficient	Constant shear friction/0.12

3. COLD FORMING OF STAINLESS BATTERY BOLTS

A numerical study is carried out for the multi-stage cold forming of square head bolts through five stages. The effects of forming force responses, maximum forming loads, effective stresses and effective strain distributions, and metal flow patterns are investigated.

3.1 The Forming Load Response and Deformation Energy

The five-stage forming simulation results are shown in Figure 3 for the axial forces. The maximum forming forces are indicated for each stage. The axial forming stroke (ΔL) and deformation energy (E) for each stage are listed in Table 3. For the force responses of forming force during all stages, it is observed that at first stage the maximum axial forming force is 75.5 kN, where there is only a minor deformation to remove the sharp cutting edges and to center for the backward extrusion. Thus, the acted axial forging stroke is only 2.00 mm and the forming energy is 36.8 J, as shown in Table 3. In the second stage, the maximum forming force increased to 50.7 kN to backward extrude over the die pin, with a reduction in area of 25.6% to form the cavity of ϕ3.0 mm with 5.0 mm depth. The acted axial forging stroke is 4.11 mm and the forming energy is 128.5 J, as shown in Table 3.

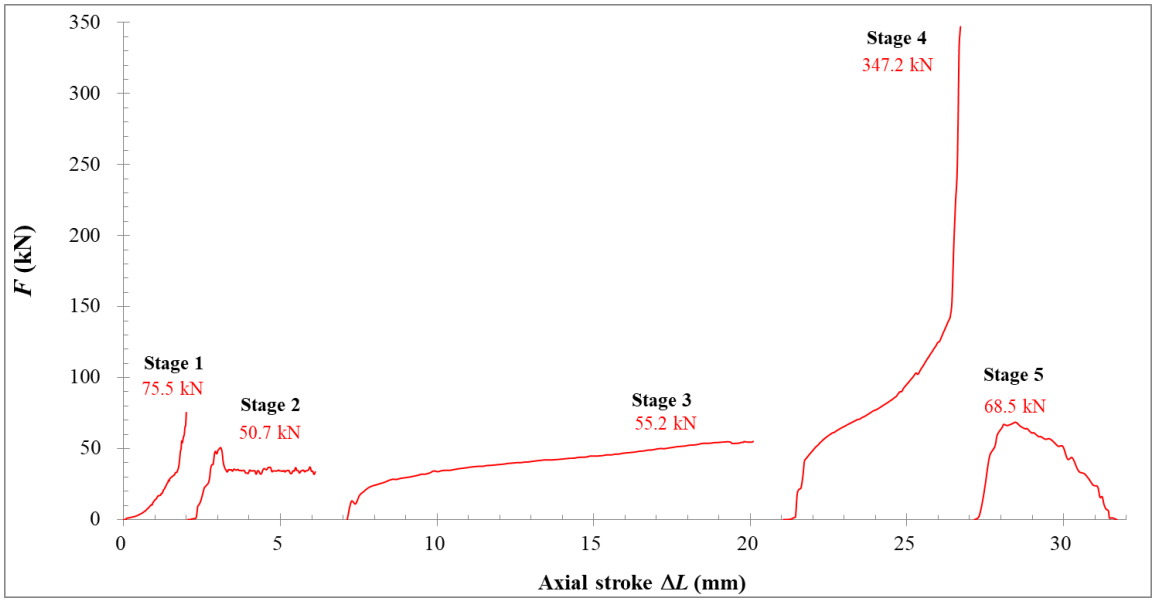

Figure 3: Axial Forging responses for five-stage forming.

In the third stage, it firstly upsets a head into a conical shape in the maximum forming force at 55.2 kN, as shown in Figure 3, and the forming energy of 530.1 J, as shown in Table 3, which is the greatest of the five stages due to longer acted axial forming stroke of 13.09 mm. In the fourth stage for the secondary upsetting into an approximately cylindrical shape with a height of 4 mm, the maximum axial forming force is increased to 347.2 kN, which is the greatest of the five stages and is more than six times that of the third stage, while the forming energy of 468.8 J is smaller than that of the third stage but larger than those of the first and second stages, as shown in Table 3. At the last stage, the head of the workpiece is trimmed into a thick square shape and the maximum axial forming force is 68.5 kN, as shown in Figure 3, while the

forming energy of 191.7 J is smaller than those of the third and fourth stages due to shorter acted axial forming stroke, as shown in Table 3.

For the maximum axial forming force, as shown in Figure 3, the fourth stage, which the head of the workpiece is secondary upset into an approximately cylindrical shape with a height of 4mm (Figure 1), is the largest among the five stages. For the forming energy, as shown in Table 3, the third stage, which the workpiece is firstly upset into a conical shape (Figure 1), is the largest among the five stages due to longer acted axial forming stroke. Overall, the total maximum axial forming forces from the first to the last stages are 597.1 kN; and the total forming energies shown in Table 3 are about 1.36 kJ.

Table 3: The acted axial forging stroke (ΔL) and deformation energy (E) for each stage.

Stage	1	2	3	4	5	Total
E (J)	36.8	128.5	530.1	468.8	191.7	1,355.9
ΔL (mm)	2.00	4.11	13.09	5.71	4.70	

3.2 The Effective Stress Analysis

The effective stress distributions are shown in Figure 4 at the final position of each stage for the five-stage forming, and the maximum effective stresses are indicated.

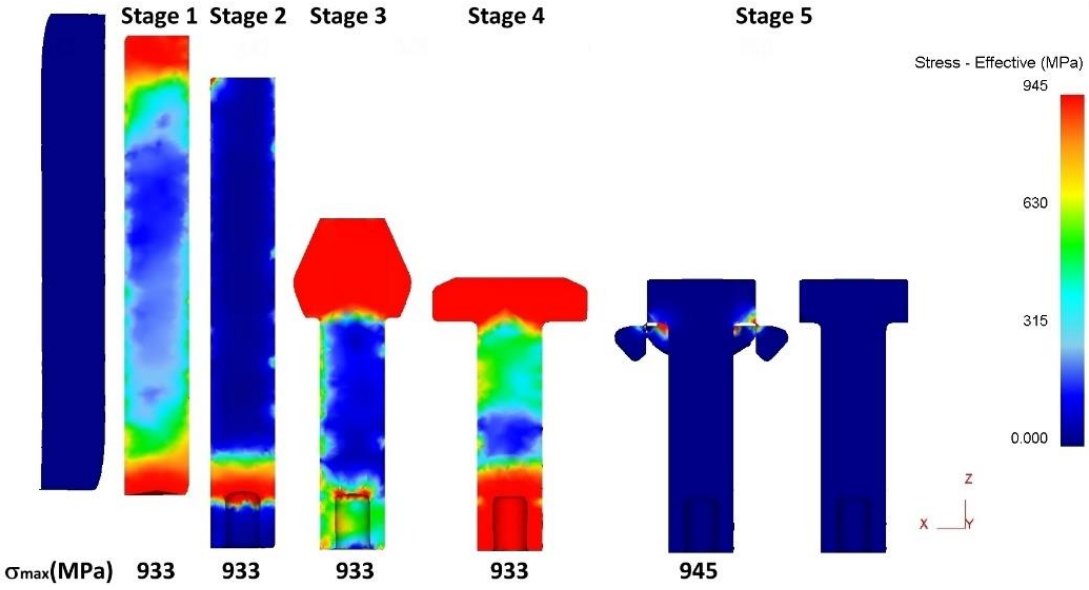

Figure 4: The effective stress distributions at the final position of each stage.

For the first stage, stresses are arising at the upper and lower ends of workpiece when they are in contact with the dies, then the stresses increase as the forging load increases, the maximum effective stress is 933 MPa. It is observed that the highest value of effective stress occurs in the upper and lower ends whereas the lowest value of effective stress occurs in the middle region of workpiece. For the second stage which involves backward extrusion over a die pin, it is analyzed from Figure 4 that the effective stresses are high in the extrusion deformation region. This leads to the formation of a cavity at lower face under high pressure

in turn causes high effective stress of 933 MPa on workpiece and tool surface. The stress response in the backward extrusion region of workpiece is obviously larger, as shown in Figure 4. For the third stage which involves the firstly upsetting into a conical shape, stresses are arising in the upsetting region and at the lower end of workpiece when they are in contact with the dies, then the stresses increase as the forming load increases, the maximum effective stress is 933 MPa. It is observed that the highest value of effective stress occurs in the upsetting region and at the top end of bottom cavity whereas the lowest value of effective stress occurs in the middle region of workpiece.

In the fourth stage, the head of the workpiece is secondary upset into an approximately cylindrical shape with a height of 4 mm. As the punch stroke increasing, axisymmetric upsetting formation begins. The stress response is significantly larger for almost the head of workpiece, as shown in Figure 4. The maximum effective stress is 933 MPa. In the fifth stage, the process of trimming over a moving punch is carried on to form a thick square head. This results in a shear formation of the square head in the upper face under high pressure, resulting in high effective stress of 945 MPa, as shown in Figure 4.

3.3 The Effective Strain Analysis

Figure 5 shows the effective strain distributions at the final position for the five stages. In the first stage, the effective strains in flatting (upper) and centering (lower) regions of workpiece are higher than the middle region where the deformation is small, as shown in Figure 5. The effective strain distributions are not completely symmetric due to the visible deformation to the ends of the cutoff billet. For the second stage of backward extrusion over a die pin at the lower end, the effective strains are high in the upper end and the region of backward extrusion forming with large deformation, as shown in Figure 5. The region with higher effective strains increases along the die pin due to the friction resistance on the contact surfaces between die pin and workpiece.

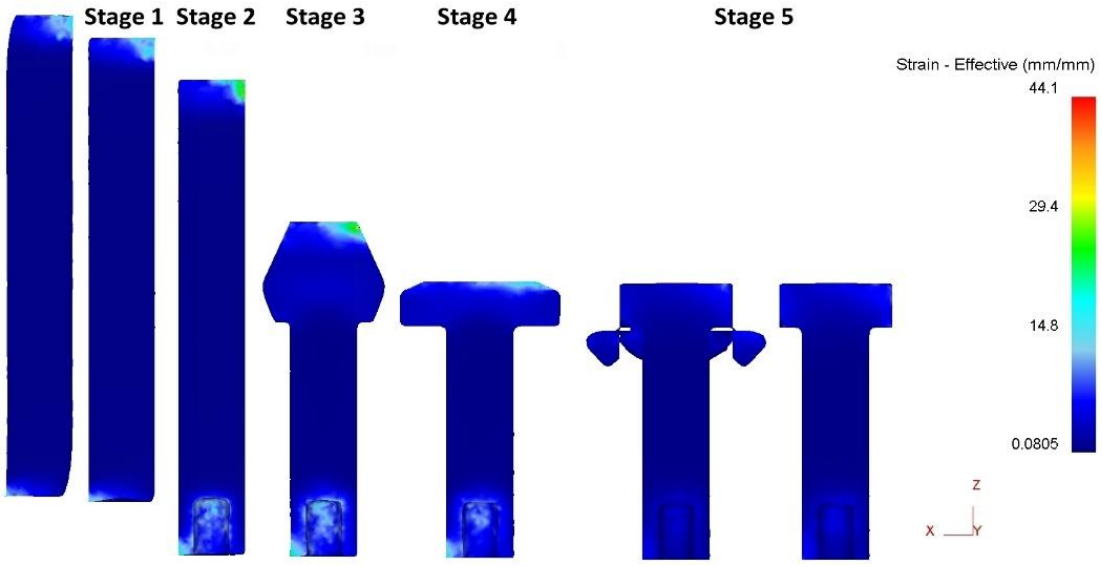

Figure 5: The effective strain distributions at the final position of each stage.

For the third stage of the firstly upsetting into a conical shape over a punch, the effective strains are high in the upsetting region with large deformation and in the lower region compression over a die pin. For the fourth stage of secondary upsetting the upper head of the workpiece, the effective strains are obviously high in the upsetting zone and the lower region compression over a die pin, while the effective strains of the other region are relatively small, as shown in Figure 5. However, even if the first four stages are axisymmetric forming, their effective strain distributions are obviously not axisymmetric, as shown in Figure 5, since the initial billet is not an axisymmetric cylindrical body. In the fifth stage, the process of trimming over a moving punch is conducted to form a thick square head and the effective strains are higher in the trimming region, while the effective strains of the other region are relatively small, as shown in Figure 5.

3.4 The Flow Line Analysis

When the metal is deformed by cold forming, the deformed grains and inclusions in the metal distribute in bands along the main deformation direction of the metal to form the grain flow lines. The simulation results of flow lines, as shown in Figure 6, for the five-stage forming. The flow lines in the initial billet are almost evenly distributed, as shown in Figure 6, except at both ends where the flow lines are vertically bent and highly compacted due to shear deformation. Highly compacted flow lines indicate higher hardness [17].

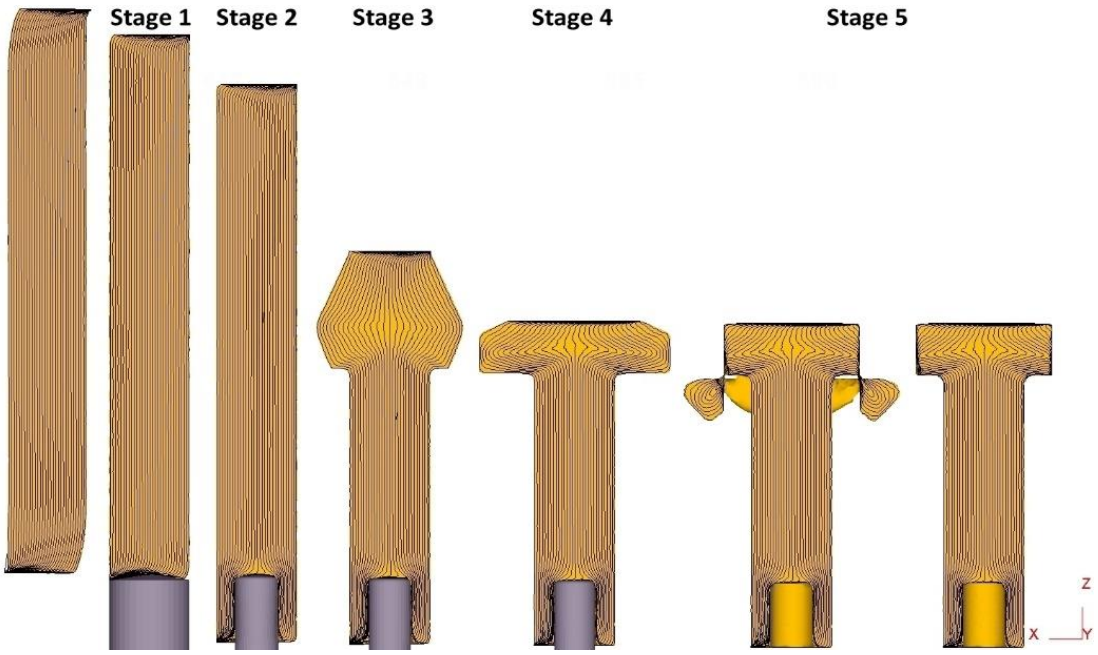

Figure 6: The simulation results of flow lines at the final position of each stage.

In the first stage, the flow lines in flatting and centering regions of workpiece are highly compacted, while in the middle region with low deformation, the flow lines are almost evenly distributed. For the second stage of backward extrusion over a die pin at the lower end, the flow lines in the inner wall of the lower cavity are obviously highly compacted, as shown in Figure 6, because of severe structure deformation. In the third stage, the flow lines in the upper and lower regions of upsetting head are curved and highly compacted, as shown in

Figure 6. For the fourth stage of secondary upsetting the upper head of the workpiece, the flow lines in upsetting zone of workpiece are heavily curved and those in the bottom region of the head are more highly compacted, as shown in Figure 6.

For the fifth stage of trimming to form a square head, the flow lines in the trimming region of the head are severely bent, highly compacted, fractured due to heavily trimming, and eventually, the flow lines near the edge of the head are torn to break, as shown in Figure 6.

4. CONCLUSIONS

A multi-stage cold forming process for the manufacture of stainless battery bolts is studied numerically with AISI 316 stainless steel. The cold forming process through five stages includes preparation and centering for backward extrusion, backward extrusion over die pin, two upsetting operations, and square trimming. The numerical simulations of cold forming are carried out using the finite element code of DEFORM-3D. The formability of the workpiece is studied, such as the effect on forming force response, maximum forming force, effective stress and strain distributions, and metal flow pattern.

For the maximum axial forming force, the fourth stage of secondary upsetting to form a cylindrical head to a larger outer diameter is 347.2 kN, which is the largest among the five stages due to the large amount of upsetting. However, for the forming energy, the third stage, which the workpiece is firstly upset into a conical shape, is 530.1 J, which is the largest among the five stages due to longer acted axial forming stroke. Overall, the total maximum axial forming forces from the first to the last stages are 597.1 kN and the total forming energies are about 1.36 kJ.

In the five-stage forming process, in the two upsetting and the square trimming forming stages, the effective stresses in the head of the workpiece are significantly high, and the effective strains are also significantly high due to large deformation. In particular, the maximum effective stress in the fifth stage, the process of trimming to form a thick square head, is 945 MPa, which is the largest among the five stages. The flow line distributions are also very complex in which the flow lines in the trimming region of the upset head are severely bent, highly compacted, and eventually fractured due to excessive trimming. However, even if the first four stages are axisymmetric forming, their effective strain and flow line distributions are obviously not axisymmetric since the initial shearing billet is not an axisymmetric cylindrical body.

REFERENCES

[1] Padfield, T. and Bhupatiraju, M., Cold heading. In Metalworking: Bulk forming, ASM International: Materials Park, OH, USA, 2008.

[2] Altan, T. and Knoerr, M., Application of the 2D Finite Element Method to Simulation of Cold Forging Processes. Journal of Materials Processing Technology, 1992. 35: p. 275–302.

[3] Lee, J.-H.; Kang, B.-S.; Lee, J.-H., Process design in multi-stage cold forging by the finite-element method. Journal of Materials Processing Technology, 1996. 58(2-3): p. 174-183.

[4] Joun, M.S.; Lee, S.W.; Chung, J.H., Finite element analysis of a multi-stage axisymmetric forging process. International Journal of Machine Tools and Manufacture, 1998. 38: p. 843-854.

[5] Roque, C.M.O.L. and Button, S.T., Application of the finite element method in cold forging processes. Journal of the Brazilian Society of Mechanical Sciences, 2000. 22(2): p. 189-202.

[6] MacCormack, C. and Monaghan, J., 2D and 3D finite element analysis of a three stage forging sequence. Journal of Materials Processing Technology, 2002. 127: p. 48–56.

[7] Park, K.S.; VanTyne, C.J.; Moon, Y.H., Process analysis of multistage forging by using finite element method. Journal of Materials Processing Technology, 2007. 187–188: p. 586-590.

[8] Farhoumand, A. and Ebrahimi, R., Analysis of forward–backward-radial extrusion process. Materials & Design, 2009. 30: p. 2152-2157.

[9] Jafarzadeh, H.; Faraji, G.; Dizaji, A.F., Analysis of lateral extrusion of gear-like form parts. Journal of Mechanical Science and Technology, 2012. 30: p. 3243-3252.

[10] Paćko, M.; Sleboda, T.; Macioł, S.; Packo, P., Optimization of a Bolt Forming Process by Means of Numerical Simulation. Steel Research International, 2012.

[11] Yang, C.-C. and Lin, X.-Y., The Forming Analysis of Two-stage Extrusion for 1010 Fastener. Journal of Mechanical Engineering and Automation, 2016. 6: p. 43-45.

[12] Ku, T.-W., A Study on Two-Stage Cold Forging for a Drive Shaft with Internal Spline and Spur Gear Geometries. Metals, 2018. 8(11), 953.

[13] Francy, K.A.; Rao, C.S.; Gopalakrishnaiah, P., Optimization of Direct Extrusion Process Parameter on 16MnCr5 and AISI1010 Using DEFORM-3D. Procedia Manufufacturing, 2019. 30: p. 498-505.

[14] Obiko, J.O.; Mwema, F.M.; Bodunrin, M.O., Finite Element Simulation of X20CrMoV121 Steel Billet Forging Process Using the Deform 3D Software. SN Applied Sciences, 2019. 1(9).

[15] Petkar, P.M.; Gaitonde, V.N.; Karnik, S.R.; Kulkarni, V.N.; Raju, T.K.G.; Davim, J.P., Analysis of Forming Behavior in Cold Forging of AISI 1010 Steel Using Artificial Neural Network. Metals, 2020. 10(11), 1431.

[16] Lee, H.-S.; Park, S.-G.; Hong, M.-P.; Kim, Y.-S., Process design of multi-stage cold forging with small size for ESC solenoid valve parts. Journal of Mechanical Science and Technology, 2022. 36: p. 359-370.

[17] Yang, C.-C. and Liu, C.-H., The Study of Multi-Stage Cold Forming Process for the Manufacture of Relief Valve Regulating Nuts. Applied Sciences, 2023. 13(10), 6299.

[18] Yang, C.-C.; Sumampow, Y.; Cruz, S.N.D., The Cold Forming Analysis of Eccentric Parts. European Journal of Applied Sciences, 2023. 11(3): p. 407-421.

[19] Tao, L.; Feng, Z.; Jiang, Y.; Tong, J., Analyzing Forged Quality of Thin-Walled A-286 Superalloy Tube under Multi-Stage Cold Forging Processes. Materials, 2023. 16, 4598.

[20] Wan, N.; He, Q.; Jing, X.; Jiang, Y.; Zhou, H., Numerical and experimental investigation of the effect of cold extrusion process on residual stress and fatigue life of internal threadof high-strength steel. The International Journal of Advanced Manufacturing Technology, 2023. 127: p. 4713–4726.

[21] Yang, C.-C.; Nguyen, T.V.; Andres, J.C., The Cold Forming Analysis of Stainless Steel Socket-Head Screws. European Journal of Applied Sciences, 2023. 11(6): p. 225-237.

[22] Winiarski, G.; Gontarz, A.; Skrzat, A.; Wójcik, M.; Wencel, S., Analysis of a New Process for Forming Two Flanges Simultaneously in a Hollow Part by Extrusion with Two Moving Dies. Metals, 2024. 14(6), 612.

[23] Hosford, W.F., Mechanical Behavior of Materials, Cambridge University, NY, USA, 2005.